eprints@whiterose.ac.uk
https://eprints.whiterose.ac.uk/

AeroTail: A Bio-inspired Aerodynamic Tail Mechanism for Robotic Balancing

Jingcheng Sun and Chengxu Zhou

Abstract—This paper presents a novel bio-inspired "tail" design that harnesses aerodynamic drag to generate torque for robotic balancing. Drawing inspiration from the natural world, this innovative approach aims to improve the efficiency of balancing robots while reducing their overall mass. While reaction wheels have been widely used for satellite stabilisation and inverted pendulum-like balancing robots, their inherent mass can be problematic in Earth's environment. Biomimetic research demonstrates that animal tails can produce torque for righting and manoeuvring during rapid movement due to their aerodynamic features, such as fur. Motivated by these observations, we proposed a bio-inspired tail mechanism that balances robots by exclusively utilising aerodynamically induced torques. To simulate this device, an inverted pendulum-based dynamic model is introduced, and the balancing process is governed by a PD controller. Comparative simulation studies examine the behaviours of a traditional reaction-wheel-based tail (RW tail) and the proposed aerodynamic drag-driven tail (AeroTail), discussing their respective advantages and limitations. The findings reveal that the AeroTail outperforms the RW tail in most metrics, achieving a remarkable 33.2% reduction in peak torque input and a 72.8% decrease in peak velocity requirement while not relying on extra mass to function.

I. INTRODUCTION

Contemporary machines and devices, such as drones, satellites, legged robots, rockets, and underwater vehicles, necessitate active re-orientation and attitude error correction to maintain balance. These machines perform critical tasks, including telecommunications, inspection, cargo delivery, and access to non-human-friendly environments. To fulfil their intended functions, adherence to specific payload requirements and limitations is paramount. Thus, it is essential that additional, yet necessary payloads, such as balancing mechanisms, are minimised.

Various balancing methods exist for these devices and vehicles, with reaction wheels being the most widely used approach. Employing inertial forces to provide balancing torques, reaction wheels are particularly prevalent in satellite applications, where external forces are challenging to obtain in space [1]. In robotics, reaction wheels have also been utilised for balancing and re-orientation purposes. Research in this area frequently employs dynamic models based on

the inverted pendulum [2], with a primary focus on control. One such study [3] introduces a dynamic model for balancing robots on a point-in-plane and demonstrates an example robot that utilises a reaction wheel-style crossbar for balance. The Cubli [4], a cube-shaped robot with three reaction wheels controlling each axis, is capable of jumping up and balancing on a corner. Another popular method for robotic balancing is utilising propellers facing a perpendicular plane thus generating torque from their thrust. Notable examples include Salto [5], the slackliner robot [6], and LAWCDR [7]. Although these solutions offer some advantages, they suffer from the additional mass and structural complexity that could be otherwise reserved for their primary functions. Furthermore, unlike satellites, terrestrial robots have ample means to generate external forces for balance, and therefore, using inertial balancing as the default option may not be well justified.

Inspiration for alternative balancing mechanisms can be found in nature, where animals utilise their tails for balance during activities such as jumping and running due to evolutionary pressures [8]. Researchers have investigated the balancing role of tails and appendages in animal behaviours, including running, jumping, and self-righting [9]. Others have developed dynamic models and control systems to integrate biomimetic tail mechanisms into robots [10]. A study by [11] found that an increased tail-to-body length ratio in geckos results in a significant rise in turning rate, but the benefits of a longer tail rapidly diminish with a larger ratio. Thus, animal tails can be used effectively in a reaction-wheel manner, albeit with limitations.

Certain animal tails possess surface properties, typically due to fur or feathers, which enable them to induce aerodynamic drag when moving. The Cheetah's tail inspires a simplified tail device that swings in a conical motion during turns [12], achieving 70% more lateral acceleration with a tail than without one. Wind tunnel tests quantify the aerodynamic forces on the tail, revealing that the fur nearly doubles the effective frontal area [13]. The aerodynamic effects contribute to the angular impulse imparted by the tail onto the cheetah's body. In these experiments, aerodynamic torque surpasses inertial torque as the tail accelerates at around 0.05 s, albeit with diminishing increments thereafter. The results show that 26% of the pitch angular impulse is induced aerodynamically even though the tail only takes 2.5% of the body mass [14]. A study by [15] demonstrates that a squirrel's bushy tail, despite comprising just 3% of the body mass, has a projected area that can reach around 55% of the body size in a side view during jumping. The aerodynamic torque produced by the tail

1

is smaller but comparable to the inertial torque.

These animal-related studies suggest that although animals can balance using their tails in a purely inertial manner, tails with aerodynamic properties significantly enhance the generated righting torque. In some cases, the aerodynamic torque induced by the tail even exceeds that produced by its inertia, suggesting that a tail's torque-generating capability could be derived entirely from its aerodynamic properties, rather than its mass. Consequently, it is theoretically possible to design a mass-less robot-balancing tail that relies solely on its aerodynamic nature to generate righting torques, thus addressing the problem of unjustified additional payload from reaction wheel mass.

In light of these findings, the primary contributions of this paper are as follows:

- Development of a robotic tail (AeroTail) device design capable of self-righting and balancing on a point-in-plane aerodynamically.
- Introduction of simplistic mathematical models based on the inverted pendulum (IP) and control methods suitable for balancing the proposed AeroTail.
- Computational simulations and comparison studies to quantify and visualise the advantages of the AeroTail mechanism over traditional reaction-wheel-based (RW) tails under various circumstances.

This paper is organised as follows: Section II presents the mathematical model and the control method, accompanied by visual illustrations; Section III-A describes the generalised AeroTail behaviour and provides an initial comparison with RW tails; Section III-B comprises four scenario tests with controlled variables, comparing the performance of both mechanisms in specific situations; and finally, further discussions and conclusions are presented in Section IV.

II. MATHEMATICAL MODELLING

To design and simulate a robot-balancing tail device, a dynamic model of the device and a simplified robot must be established. This model should be general enough to represent most scenarios where the tail is expected to be used. As mentioned in Section I, studies regarding reaction wheels often build their dynamic models based on the inverted pendulum (IP); its structure can be described as a massed object whose gravity does not align with its contact point with the surroundings. This means that most devices, especially legged robots, which require active balancing, can be well represented by the IP model. The example robot mentioned in [3] utilises a dynamic model for balancing on a point-in-plane, which simplifies the IP balancing problem to a degree that is suitable for simulation but still representative of wider scenarios. Therefore, the dynamic model for this work will primarily be based on the point-in-plane concept for IP, and further mechanisms will be developed on top of it.

A. The inverted pendulum model

The structure and notation of the double-rod pendulum system are shown in Fig. 1. The model consists of three
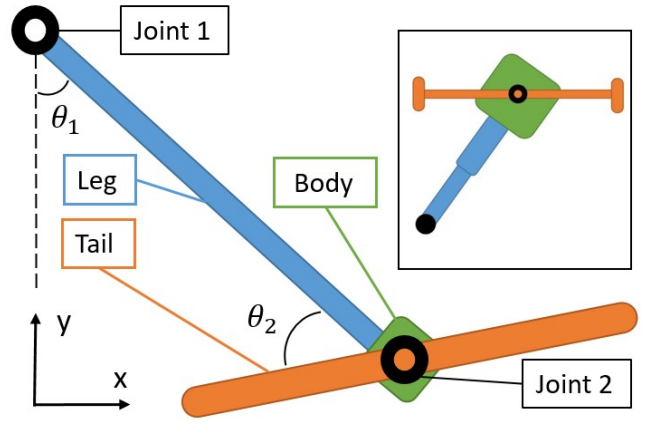

Fig. 1. The double-rod pendulum system. θ_1 is the angle between the vertical hanging position and the leg, while θ_2 is that between the leg and the tail in the same direction. The small picture in the top-right corner is an example jumping robot with equivalent components marked in the same colour as in the model.

main components: the "leg" (blue), the "body" (green), and the "tail" (orange). The leg and the body are fixed together; they both rotate around Joint 1 which connects a fixed point in the world frame with the leg. Joint 2 connects the mid-point of the tail to the body. Both the leg and the tail are uniform and rigid rods, and the body is a point mass. The masses of the leg, tail and body are m_1, m_2 and m_3 respectively. The leg has a length of $2l_1$ while that of the tail is $2l_2$. In the top right corner of Fig. 1 is a simple illustration of a monopedal jumping robot. The equivalent components in the double-rod model and the example robot are marked with the same colour. Compared to a realistic robot, the body in the model is largely simplified; Joint 1 can be seen as the contact point between the robot and the ground.

The equation of motion for the system can be simply expressed using the robot dynamics equation:

$$\mathbf{M}(\theta)\ddot{\theta} + \mathbf{C}(\theta,\dot{\theta})\dot{\theta} = \boldsymbol{\tau}_g(\theta) + \mathbf{u} + \mathbf{J}^{\mathbf{T}}(\theta)\boldsymbol{\lambda} \qquad (1)$$

in which θ, $\dot{\theta}$, and $\ddot{\theta}$ represent the positions, velocities, and accelerations of the pendulums as shown in Fig.1, the $\mathbf{M}(\theta)$ is the mass matrix, $\mathbf{C}(\theta,\dot{\theta})\dot{\theta}$ is the Coriolis forces, $\boldsymbol{\tau}_g(\theta)$ is the gravity vectors, $\mathbf{u}$ represents the control input and $\mathbf{J}^{\mathbf{T}}(\theta)\boldsymbol{\lambda}$ denotes the sum of external forces. The first three components can be derived using Lagrangian mechanics:

$$\frac{d}{dt}\frac{\partial T(\dot{\theta})}{\partial \dot{\theta}_i} - \frac{\partial U(\theta)}{\partial \theta_i} = \boldsymbol{\tau}_i. \qquad (2)$$

where $T(\dot{\theta})$ and $U(\theta)$ are the kinetic and potential energy of the system, $\boldsymbol{\tau}_i$ is the sum of external forces.

The total kinetic energy of the system is:

$$\begin{aligned} T(\dot{\theta}) =& \frac{1}{2}I_1\dot{\theta}_1^2 + \frac{1}{2}I_2(\dot{\theta}_2 + \dot{\theta}_1)^2 + \frac{1}{2}(m_2 + m_3)v_2^2 \\ =& \frac{2}{3}m_1 l_1^2 \dot{\theta}_1^2 + \frac{1}{6}m_2 l_2^2 (\dot{\theta}_2 + \dot{\theta}_1)^2 \\ & + 2(m_2 + m_3)l_1^2 \dot{\theta}_1^2. \end{aligned} \qquad (3)$$

where I_1, I_2, and I_3 are the moments of inertia for the leg, the tail, and the motor.

The total potential energy of the system is:

$$
\begin{aligned}
U(\boldsymbol{\theta}) =& m_1 g y_1 + m_2 g y_2 \\
=& - m_1 g l_1 \cos\theta_1 - 2(m_2 + m_3) g l_1 \cos\theta_1.
\end{aligned}
\tag{4}
$$

where y_1 and y_2 are the displacements of the motor and the centre of mass of the leg from Joint 1 on the y-axis.

Substitute (3) and (4) into the Lagrangian model (2), and the external forces can be expressed as a function of the pendulum state. Consequently, the mass matrix in (1) can be derived as:

$$
\mathbf{M}(\boldsymbol{\theta}) = \begin{bmatrix} \frac{4}{3}m_1 l_2^2 + 4(m_2 + m_3)l_1^2 & \frac{1}{3}m_2 l_2^2 \\ \frac{1}{3}m_2 l_2^2 & \frac{1}{3}m_2 l_2^2 \end{bmatrix}.
\tag{5}
$$

Note that the mass matrix is independent to position (θ). There are no Coriolis forces involved in the model, thus:

$$
\mathbf{C}(\boldsymbol{\theta}, \dot{\boldsymbol{\theta}}) = \begin{bmatrix} 0 & 0 \end{bmatrix}^T
\tag{6}
$$

and the gravity vectors can be expressed as:

$$
\boldsymbol{\tau_g}(\boldsymbol{\theta}) = \begin{bmatrix} gl_1 \sin\theta_1 (m_1 + 2m_2 + 2m_3) & 0 \end{bmatrix}^T
\tag{7}
$$

B. The RW tail version of the model

When the tail is acting as an RW tail, it has mass, and there are no external forces involved. Since only joint 2 will be actuated, the control input u in (1) can be written as:

$$
\mathbf{u} = \begin{bmatrix} 0 & \tau_{\text{motor}} \end{bmatrix}^T
\tag{8}
$$

and the sum of external forces is:

$$
\mathbf{J^T}(\boldsymbol{\theta})\boldsymbol{\lambda} = \begin{bmatrix} 0 & 0 \end{bmatrix}^T
\tag{9}
$$

C. The AeroTail version of the model

When the tail is behaving as an AeroTail, there are several changes to the model compared to that of the RW tail scenario. First of all, the tail is assumed to be mass-less in order to eliminate the inertial torque from the mass of the tail; thus, the new expressions for the mass matrix and the gravity vectors are:

$$
\begin{aligned}
\mathbf{M}(\boldsymbol{\theta}) &= \begin{bmatrix} \frac{4}{3}m_1 l_2^2 + 4m_3 l_1^2 & 0 \\ 0 & 0 \end{bmatrix}, \\
\boldsymbol{\tau_g}(\boldsymbol{\theta}) &= \begin{bmatrix} gl_1 \sin\theta_1 (m_1 + 2m_3) & 0 \end{bmatrix}^T.
\end{aligned}
\tag{10}
$$

The sum of aerodynamic forces generated by the tail can be seen as a concentrated external torque acting on its centre of mass. Since the tail is theoretically the "end effector" in the dynamic model, the matrix of the aerodynamic torque (τ_{aero})is expressed as such:

$$
\mathbf{J^T}(\boldsymbol{\theta})\boldsymbol{\lambda} = \begin{bmatrix} -\tau_{\text{aero}} & -\tau_{\text{aero}} \end{bmatrix}^T.
\tag{11}
$$

In this scenario, the aerodynamic torque is always equal to the motor torque, and the tail is always rotating at a constant velocity with no acceleration process when the velocity changes from one to another.

Generally, the aerodynamic drag can be calculated using the equation:
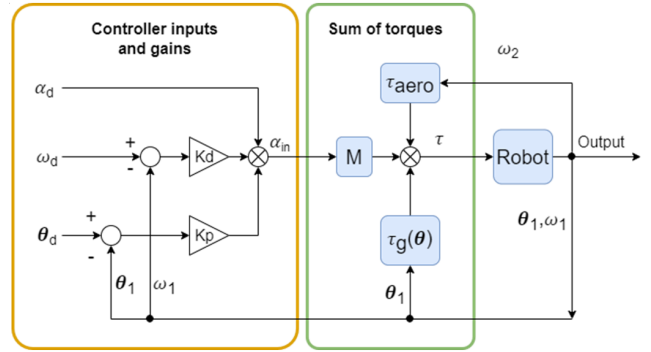
$$
D = \frac{1}{2}\rho C_D v^2 A
$$

Fig. 2. The control block diagram of the balancing model. In the diagram, α means acceleration, ω means velocity and θ represents angle position. Designation "1" is that of the body, "2" is for the tail and "d" means the desired target input.

where D is the drag force, ρ is the air density, C_D is the drag coefficient, v is the air speed and A is the frontal area. If the aerodynamic drag acts as a torque on a single point, the torque can be calculated using the method provided in [16] with the equation:

$$
\begin{aligned}
|\tau_D| &= \int_A Dl\, dA \\
&= \int_{L_1}^{L_0} \frac{1}{2}\rho C_D a(\omega l)^2 l\, dl
\end{aligned}
\tag{12}
$$

where l is the length of the lever on which the drag force exerts, a is the width of the drag inducer, ω is the angular velocity of the tail, and $L_0 - L_1$ is the length of the lever that can generate drag assuming the drag-inducing device has a uniform cross-section along its entire length.

To adapt this equation to the double-rod system, it needs to be modified and simplified. The aerodynamic torques generated by the tail originate from the drag inducers on the tail's ends; thus, the drag generated by a single inducer is considered to act on the endpoint of the tail, regardless of its own geometry, in order to simplify the model. Consequently, Equation (12) can be rewritten as:

$$
\tau_D = \frac{1}{2}\rho C_D \omega^2 l^3 A
\tag{13}
$$

where A is the area of one drag inducer. Since there are two of them on each end of the tail, the actual aerodynamic drag generated by the tail is $\tau_{\text{aero}} = 2\tau_D$.

D. Control method

The control method employed for the model is a classic Proportional-Derivative (PD) controller, commonly used for balancing inverted pendulums. Fig. 2 depicts the control block diagram of the model, in which the controller gains are represented by K_p (proportional gain) and K_d (derivative gain). his controller facilitates the balancing of the robot at a desired angle (θ_d) and target velocity (ω_d). Given that the proportional term contains the position angle error of the robot body, the derivative term error can be easily derived from
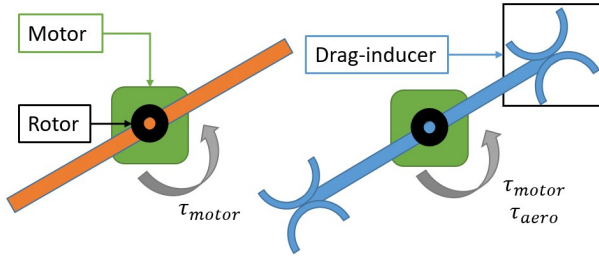
Fig. 3. The tail models for the stand-alone tests. The motors are fixed to the world frame; the RW tail (orange) and the AeroTail (blue) have the same length. The grey arrows point out the torques acting on the tails. In the top-right box is one of the drag-inducers which generates aerodynamic torque when the tail is rotating; it can be seen as a semi-circle prism.

TABLE I
PARAMETERS OF THE TAIL STAND-ALONE TESTS

Definition	Designation	Parameter
RW tail mass	m_I	10 g
AeroTail mass	m_D	varies
Half-tail lengths	l	5 cm
Rotor mass	m_R	5 g
Motor-torque	τ_{motor}	0.01 Nm
Aero-torque	τ_{aero}	varies
Drag coefficient	C_D	2.0

the feedback velocity. Consequently, the expression for the summed acceleration input can be formulated as:

$$\alpha_{in} = K_p(\theta_d - \theta_1) + K_d(\omega_d - \omega_1), \quad (14)$$

where θ_1 and ω_1 represent the real-time position angle and velocity of the body, respectively. The integral gain is not required, as there is no noise in the simulation environment. The controller also accounts for gravity and mass, allowing the input to be acceleration rather than torque. As a result, comparative studies in the simulation phase with fixed gains are possible, and altering the mass of components will not affect the robot's result trajectory, provided the gains remain constant.

III. SIMULATION STUDIES

The simulation of the proposed theoretical model is performed using MATLAB. The simulation codes involve iterative calculations employing Euler's method.

A. Tails stand-alone tests

An RW tail will be compared to an AeroTail to examine their behaviours under the same conditions. The controlled variables are as follows:

- Identical motors must be used;
- The lengths of the tails must be the same.

The term "stand-alone" in this section refers to both mechanisms operating without the body. Fig. 3 presents the theoretical models for the tail stand-alone tests. The black circles in the middle of the rods symbolise the motor rotors (the rotor is assumed to be a uniform disc with a diameter of 2 cm). The effective area of a drag-inducer is equal to the width of the
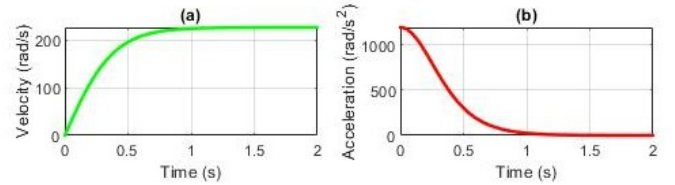

Fig. 4. The behaviour of the aero-balanced tail with mass. (a) The velocity of the tail versus time. (b) The acceleration of the tail converges to zero.
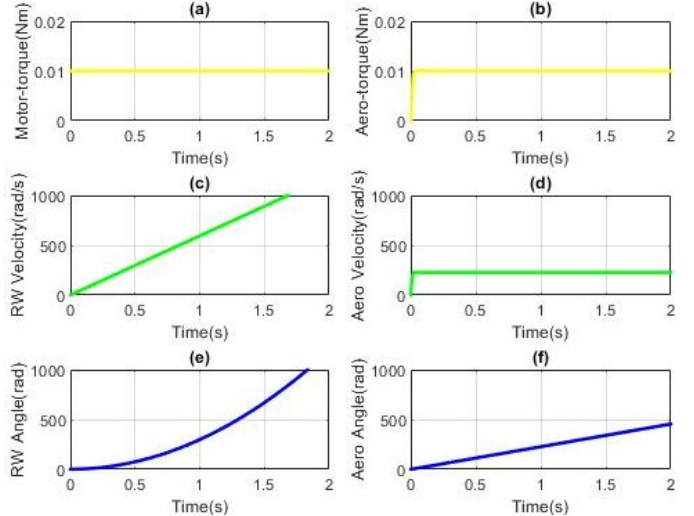

Fig. 5. The comparison between aero-balanced and reaction-wheel tails. (a) The torque provided by the motor. (b) The aerodynamic torque generated by the AeroTail. (c) & (d) The velocities of the tails versus time. (e) & (f) The angles of the tails versus time.

prism multiplied by the diameter of the semi-circle. Parameters for the simulations are detailed in Table I.

1) The behaviour of an AeroTail with mass: The first simulation aims to demonstrate the behaviour of a reaction wheel capable of generating significant aerodynamic drag from its rotation when driven by a constant torque from the motor. In this case, m_D is 10 grams and torque input is τ_{motor}. The additional τ_{aero} is calculated using the aerodynamic model in Section II-C, assuming the drag acts on the ends of the tail. The drag coefficient is 2.0, that of the semi-circle prism [16], and the contact area is set to be 5 cm^2 on each end. The simulation results are shown in Fig. 4. The acceleration of the tail eventually ceases when it reaches the maximum velocity because the torque provided by the motor equals the torque generated by drag. Unlike pure reaction wheels, which need to keep accelerating to generate torque by inertia, AeroTail can fulfil the same function with a constant velocity.

2) Comparison between AeroTail and RW tail: To compare the mechanisms, the correcting torque generated by the Aero-Tail is assumed to be predominantly aerodynamic, thus m_D is zero and the tail provides no inertial torque; simultaneously, the RW tail has no aerodynamic property in this section. Fig. 5 illustrates the comparison between the AeroTail (right) and RW tail (left), with all other conditions remaining the same.
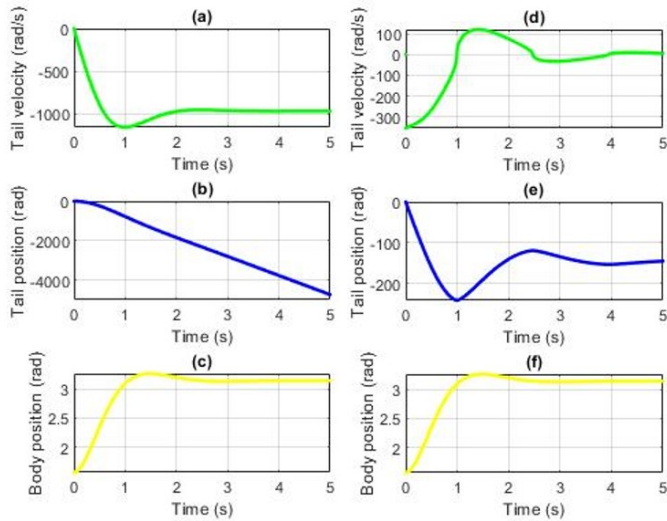
Fig. 6. Results from the example tests (RW tail on the left and AeroTail on the right): (a) & (d) The velocity of the tail reaches a constant as the system converges. (b) & (e) The position of the tail versus time. (c) & (f) The body angle reaches the target up-right position (π).

Because the AeroTail is mass-less and the inertia of the rotor is negligible, its angular velocity nearly instantaneously reaches its maximum. The net energy consumption is also calculated as the total energy output from the motor. During the test, the AeroTail used 4.53 J, while the RW tail consumed 11.99 J.

B. Scenario tests

For scenario tests, the tails will be used to balance a robot body based on the model in Section II. This implies that, unlike the stand-alone tests, the motor output during balancing will be controller-driven using the control method mentioned in the same section.

1) Example test: An example test is conducted to demonstrate the characteristics of the tails' performances. The robot (using the previous dynamic model and control method in Section II) needs to be balanced to an upright position from a $90°$ tilt within 3 seconds; the mass of the body is 20 grams, the RW tail is 10 grams, and the AeroTail is mass-less. The gains for the PD control are also determined in the example test. An additional requirement stipulates that there should only be one positive and one negative overshoot for the body position before convergence, with an error allowance of $1°$ plus or minus. The results of the example test are shown in Fig. 6. The tail's peak velocity is 355 rad/s with a net energy consumption of 4.05 J. The body positions of both tails follow identical trajectories as expected, and the RW tail experiences significantly more rotations than its counterpart. The tail velocity in (d) appears to be as smooth as other graphs because it is solely dependent on the motor torque and there is no acceleration process when the motor torque changes; it also converges to zero after the motor torque does with some delay.

Following the example tests, specific metric comparisons with controlled variables will be conducted. Four tests in

total will be performed, and the controller gains will remain constant throughout all of them.

2) Test 1: The first test compares the peak motor output torque of both mechanisms with different robot body mass (m_3). Fig. 7 (a) displays the change in peak motor torques as the robot body mass increases from 20 g to 70 g. The peak torques of both the RW tail and AeroTail rise linearly, with the RW tail's graph generally higher and exhibiting a steeper slope than the AeroTail's. To maintain constant peak velocity, the RW mass must increase with the body mass; thus, as the body mass increases, the peak torque of the RW tail grows faster than that of the AeroTail. On average, AeroTail can achieve a 33.2% reduction of peak torque input. This test demonstrates that the AeroTail offers an advantage in terms of motor torque output requirements and the potential to reduce the robot's total mass.

3) Test 2: The second test compares the peak motor velocities of both tails with varying correction angles (angles required for righting from the initial to the target position). As shown in Fig. 7 (b), the AeroTail's peak velocity remains relatively stable within the 200 to 400 rad/s range as the correction angle increases, whereas the RW tail's peak velocity triples. The AeroTail's ability to reach an ultimate velocity when exerting torque causes its peak velocity to fluctuate less when the correction angles differ significantly. This test indicates that the AeroTail has a lower requirement for peak motor velocity, consistently lower than that of the RW tail; particularly at a correction angle of $120°$, for which the AeroTail manage to achieve a peak velocity reduction of 72.8%.

4) Test 3: The third test compares the energy consumption of both mechanisms with varying tail masses (for the RW) as a percentage of the robot's body mass. The AeroTail's graph in Fig. 7 (c) is included for comparison purposes only, as it does not have mass. The AeroTail's energy consumption remains constant at 7.42 J under initial conditions (identical to the example tests), while the RW tail's energy consumption dramatically decreases as the tail mass increases from 20% to 80% of the body, intersecting the AeroTail's graph at 60%. This test reveals that the RW tail can outperform the AeroTail in some metrics even with the mass disadvantage. However, to match the AeroTail's performance, the RW tail mass must constitute 60% of the body, which is impractical if the robot needs to perform functions other than balancing.

5) Test 4: The fourth test compares the energy consumption of both tails with different correction angles. In Fig. 7 (d), the AeroTail's graph is closer to that of the RW tail, with a less pronounced curvature, resembling the results of Test 2. This indicates that the RW tail's energy consumption is more susceptible to changes in correction angles, leading to the shapes of the graphs: the outcomes for the tails are similar at very small and very large correction angles but increasingly divergent in the middle range. As with Test 2, the difference in energy consumption of the tails is greatest at a correction angle of $120°$. For most angles, the AeroTail consumes less energy to balance, rendering it superior in this metric.
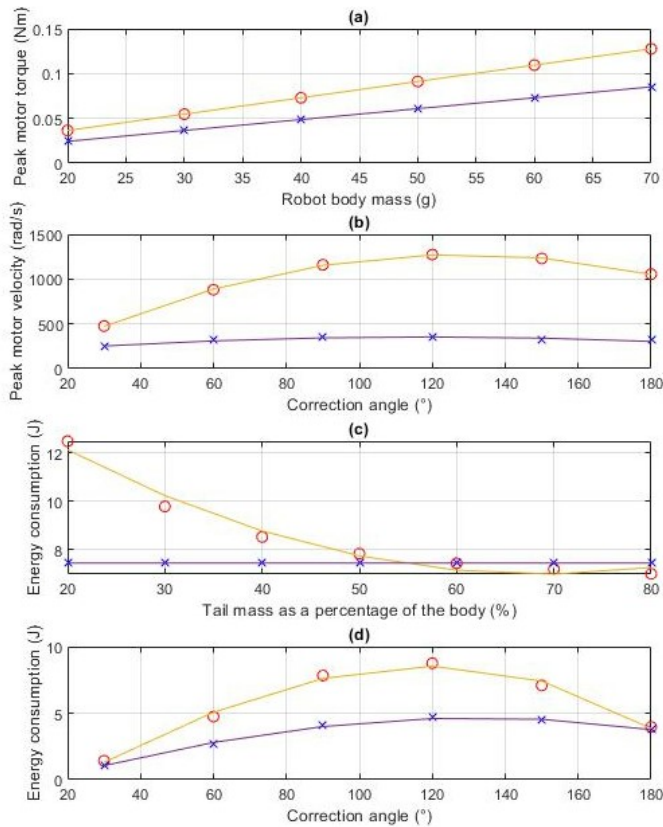
Fig. 7. The results from the 4 simulation studies: (a) Peak motor output torque versus robot body mass of RW tail and AeroTail (purple); (b) Peak velocity versus correction angle of both tails. (c) Energy consumption versus tail masses of the tails as percentages of the robot. (d) Energy consumption versus correction angles of the tails.

IV. CONCLUSION

This paper introduced the AeroTail, a robotic tail device design capable of self-righting and balancing on a point-in-plane aerodynamically. The tail mechanism's dynamic model is based on the classic IP with additional aerodynamic features, and a suitable control method for such a device was chosen accordingly. Computational simulations using MATLAB visualised and quantified the behaviour of the tails with both aerodynamic and inertial effects under various conditions and scenarios. Comparative studies with controlled variables were conducted to evaluate their performances, illustrating their respective advantages and limitations. The most significant advantage of the AeroTail over the RW tail is its lack of mass, allowing it to maintain a low increase in peak motor torque output as the robot body mass increases. Conversely, the RW tail experiences dramatically high energy consumption with a low tail-to-body mass ratio, while the AeroTail does not require mass to function.

In terms of both peak motor velocity and energy consumption, the AeroTail outperforms the RW tail when the correction angle is between the horizontal and $140°$, with the differences in results peaking at $120°$. However, the RW tail has a relative advantage at very small correction angles

or near the vertically hanging position. Future work will involve the design and construction of a physical tail device to conduct similar experiments and validate the points made in this paper. This device will utilize the same theoretical model and parameters used in the simulations. Results from physical experiments will better represent the tails' performance in realistic scenarios, and noise can be easily added to simulate the external turbulence encountered during stabilization.

REFERENCES

[1] D. Carré and P. Bertrand, "Analysis of hubble space telescope reaction wheel lubricant," *Journal of Spacecraft and Rockets*, vol. 36, no. 1, pp. 109–113, 1999.

[2] J. Meyer, N. Delson, and R. A. de Callafon, "Design, modeling and stabilization of a moment exchange based inverted pendulum," *International Federation of Automatic Control*, vol. 42, no. 10, pp. 462–467, 2009.

[3] R. Featherstone, "A simple model of balancing in the plane and a simple preview balance controller," *The International Journal of Robotics Research*, vol. 36, no. 13-14, pp. 1489–1507, 2017.

[4] M. Hofer, M. Muehlebach, and R. D'Andrea, "The one-wheel cubli: A 3d inverted pendulum that can balance with a single reaction wheel," *Mechatronics*, vol. 91, p. 102965, 2023.

[5] D. W. Haldane, J. K. Yim, and R. S. Fearing, "Repetitive extreme-acceleration (14-g) spatial jumping with salto-1p," in *IEEE/RSJ International Conference on Intelligent Robots and Systems*, pp. 3345–3351, 2017.

[6] K. Kim, P. Spieler, E.-S. Lupu, A. Ramezani, and S.-J. Chung, "A bipedal walking robot that can fly, slackline, and skateboard," *Science Robotics*, vol. 6, no. 59, p. eabf8136, 2021.

[7] C. Huang, Y. Liu, K. Wang, and B. Bai, "Land–air–wall cross-domain robot based on gecko landing bionic behavior: System design, modeling, and experiment," *Applied Sciences*, vol. 12, no. 8, p. 3988, 2022.

[8] S. Shield, R. Jericevich, A. Patel, and A. Jusufi, "Tails, flails, and sails: How appendages improve terrestrial maneuverability by improving stability," *Integrative and Comparative Biology*, vol. 61, no. 2, pp. 506–520, 2021.

[9] J. W. Young, B. A. Chadwell, N. T. Dunham, A. McNamara, T. Phelps, T. Hieronymus, and L. J. Shapiro, "The stabilizing function of the tail during arboreal quadrupedalism," *Integrative and Comparative Biology*, vol. 61, no. 2, pp. 491–505, 2021.

[10] R. Briggs, J. Lee, M. Haberland, and S. Kim, "Tails in biomimetic design: Analysis, simulation, and experiment," in *IEEE/RSJ International Conference on Intelligent Robots and Systems*, pp. 1473–1480, 2012.

[11] R. Siddall, V. Ibanez, G. Byrnes, R. J. Full, and A. Jusufi, "Mechanisms for mid-air reorientation using tail rotation in gliding geckos," *Integrative and Comparative Biology*, vol. 61, no. 2, pp. 478–490, 2021.

[12] A. Patel and E. Boje, "On the conical motion of a two-degree-of-freedom tail inspired by the cheetah," *IEEE Transactions on Robotics*, vol. 31, no. 6, pp. 1555–1560, 2015.

[13] A. Patel, E. Boje, C. Fisher, L. Louis, and E. Lane, "Quasi-steady state aerodynamics of the cheetah tail," *Biology Open*, vol. 5, no. 8, pp. 1072–1076, 2016.

[14] C. Fisher, "State estimation of a cheetah spine and tail using an inertial sensor network," Master's thesis, University of Cape Town, 2015.

[15] T. Fukushima, R. Siddall, F. Schwab, S. L. Toussaint, G. Byrnes, J. A. Nyakatura, and A. Jusufi, "Inertial tail effects during righting of squirrels in unexpected falls: from behavior to robotics," *Integrative and Comparative Biology*, vol. 61, no. 2, pp. 589–602, 2021.

[16] J. Norby, J. Y. Li, C. Selby, A. Patel, and A. M. Johnson, "Enabling dynamic behaviors with aerodynamic drag in lightweight tails," *IEEE Transactions on Robotics*, vol. 37, no. 4, pp. 1144–1153, 2021.